Journal of Sound and Vibration 329 (2010) 2532–2546

Contents lists available at ScienceDirect

Journal of Sound and Vibration

journal homepage: www.elsevier.com/locate/jsvi

Transfer matrix modeling of the vibroacoustic response of multi-materials structures under mechanical excitation

Dilal Rhazi *, Noureddine Atalla

G.A.U.S., Mechanical Engineering Department, Université de Sherbrooke, 2500 blvd Université, Sherbrooke, QC, Canada J1K 2R1

ARTICLE INFO

Article history:
Received 16 July 2009
Received in revised form
7 January 2010
Accepted 11 January 2010
Handling editor: A.V. Metrikine
Available online 9 February 2010

ABSTRACT

In several automotive and aircraft applications there is a need for simple tools to assess quickly and accurately the performance of sound packages. Statistical energy analysis (SEA) and the transfer matrix method (TMM) are examples of such methods. The used methodology (for modeling sound packages) is well validated for acoustic excitations (airborne). However, a simple and reliable methodology is still lacking for mechanical excitations (structure-borne). This work concentrates on the latter. It presents and compares three different simple approaches to model the vibration and acoustic response of a mechanically excited structure with an added noise control treatment. Various examples are presented to confirm their relevance and accuracy in comparison to more exact and costly methods, such as the finite element method. In particular, it is shown that the TMM with a size correction (FTMM) is accurate enough to eliminate the classical assumption of low coupling classically assumed in SEA modeling of sound packages and/or compute efficiently the structure-borne insertion loss of sound packages used in SEA and FEM models.

1. Introduction

Sound package components in aircrafts and vehicles in different configurations play a vital role for interior noise control. For this reason, the prediction of the acoustic and vibration behavior of a multi-layer structure, made up of homogeneous layers, is of interest to several industries.

A typical configuration consists of the prediction of the airborne response of a master structure with an attached noise control treatment in both single-wall and double-wall configurations. The transfer matrix method (TMM) is extensively used and is well validated for solving the above problem [1,2,3,4]. However, the application of the TMM has been mainly limited to acoustic excitations (plane wave or diffuse field). A few studies have been published on the use and application of the method for a structure-borne excitation. However, these studies remain scarce and incomplete. For instance, Villot et al. [5] rapidly hinted, in their paper on spatial windowing to account for size effects, to the use of the TMM to solve the response of a multi-layer structures with a mechanical excitation; but did not present application nor validation results. Guigou-Carter et al. [6] studied experimentally and numerically the performance of wood floorings in terms of impact noise induced by a tapping machine using transfer matrix approach. In their analytical model the system is modeled as an infinite multi-layer isotropic system. In a study comparing structure-borne and airborne insertion loss of sound packages added to automotive structures, Nelisse et al. [7] presented experimental results showing that the airborne insertion loss

* Corresponding author. Tel.: +1 819 821 8000x62658; fax: +1 819 821 7163.
E-mail address: Dilal.Rhazi@USherbrooke.ca (D. Rhazi).

0022-460X/$ - see front matter © 2010 Elsevier Ltd. All rights reserved.
doi:10.1016/j.jsv.2010.01.013

(ABIL) and the structure-borne insertion loss (SBIL) are very similar for highly damped structures, but did not give numerical results nor discuss the calculation of the SBIL using the TMM.

In this work three different approaches for predicting the vibroacoustic response of planar structures with attached acoustic materials under mechanical excitation are presented and compared. Special emphasis is given to a wave-based approach implemented within the transfer matrix method. In particular, a simple and computationally efficient finite size correction is introduced to accurately capture the vibration and acoustic response of the system below the structure's critical frequency. The method is compared to two other simpler methods. The first is based on SEA and the second on a modal formulation. Various examples involving single-wall and double-wall configurations are used to demonstrate the accuracy and limitations of the three methods. The finite element method is used as a reference. Moreover, the proposed methodology is used to illustrate the difference between airborne and structure-borne performance of such structures.

The specific problem of interest considers the prediction of the vibration and acoustic response of a planar master structure with an attached multi-layer sound package. The structure is assumed baffled for acoustic radiation and is excited by a point load with a random position (rain-on-the-roof type of excitation). The first approach is based on the propagation of plane waves in the main structure and the layers of the attached noise control treatment. The second uses statistical energy analysis (SEA) for the main structure and calculates an equivalent damping to account for the noise control treatment. The last approach uses a modal technique by calculating the equivalent impedance for the added treatment. In the three approaches, the TMM is used to model multi-layered noise control treatments.

This paper is divided in three main sections: the first focuses on the presentation of the three approaches, the second presents various numerical results to validate and/or highlight the limitations of the presented methods using the finite element method (FEM) as a reference. Finally, the last section shows an application comparing structure-borne insertion loss and airborne insertion loss to confirm the experimental results of Nelisse et al. [7].

2. Theory

2.1. Wave-based approach

In the first approach (referred to as the wave approach), the studied structures are assumed to be of infinite extent; they separate two semi-infinite fluids and are excited by a point load $f(x,y)$, as shown in Fig. 1. Moreover, the mechanical excitation and the response of the structure are assumed to be harmonic. In wave-number space (k_x, k_y), the load $f(x,y)$ can be represented by an infinite number of plane waves using the spatial Fourier integral transform by the following equation:

$$\begin{cases} f(x,y) = \dfrac{1}{4\pi^2}\displaystyle\int_{-\infty}^{+\infty}\int_{-\infty}^{+\infty} F(k_x,k_y)\exp[j(k_x x + k_y y)]dk_x\,dk_y \\ F(k_x,k_y) = \int_{-\infty}^{+\infty}\int_{-\infty}^{+\infty} f(x,y)\exp[-j(k_x x + k_y y)]dx\,dy \end{cases} \tag{1}$$

Using index 1 for the excitation side and 2 for the receiver side, the matrix connecting the pressure and velocity on one side of a multi-layer to those on the other side, as shown by Fig. 1, is generally written as

$$\begin{bmatrix} P_1 \\ V_1 \end{bmatrix} = \begin{bmatrix} T_{11} & T_{12} \\ T_{21} & T_{22} \end{bmatrix} \begin{bmatrix} P_2 \\ V_2 \end{bmatrix} \tag{2}$$

where T_{11}, T_{12}, T_{21} and T_{22} represent components of the global condensed transfer matrix, which are functions of the properties and nature of waves propagating in the system-layers and the inter-layers continuity equations [1]. P_1, V_1 represent pressure and velocity at the emission side and P_2, V_2 represent pressure and velocity at the receiver side of the

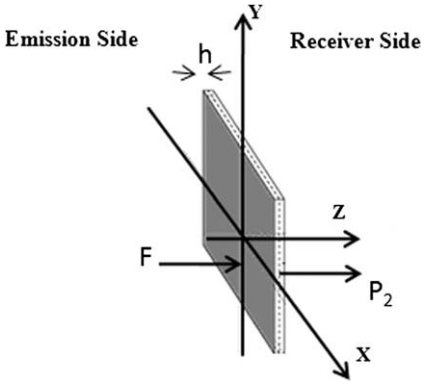

Fig. 1. Multilayered panel under mechanical excitation.

multi-layer structures. Note that the constituents transfer matrices have various dimensions and variables (e.g. solid layer will have a 4×4 matrix, a porous layer will have a 6×6 matrix….). Finally, the damping is included directly in the expression of the elastic modulus.

For each wave-number component (k_x, k_y), the transmission and radiation problems will be solved using the classic transfer matrix method. This allows for handling an arbitrary multilayer made up of a master structure (elastic, composite, sandwich, etc.) and an attached multi-layered sound package (a combination of porous, fluid, screen, etc.).

Once the various indicators (pressure, velocity, surface impedance, radiated power… etc.) are computed for a given wave-number, the global indicators are recovered using Eq. (1). For example, the quadratic velocity and radiated power of the main structure into the emission side take the form

$$\langle V^2\rangle = \frac{1}{8\pi^2 S}\int_{-\infty}^{+\infty}\int_{-\infty}^{+\infty}|[V(k_x,k_y)]_{z=0}|^2\,dk_x\,dk_y \tag{3}$$

$$\Pi_{\mathrm{rad}} = \frac{|F|^2}{8\pi^2 S}\mathrm{Re}\left[\int_{-\infty}^{+\infty}\int_{-\infty}^{+\infty}\frac{Z_{\mathrm{B},\infty}}{|Z_{\mathrm{S,TMM}}+Z_{\mathrm{B},\infty}|^2}\,dk_x\,dk_y\right] \tag{4}$$

where

$$[V(k_x,k_y)]_{z=0} = \frac{1}{Z_{\mathrm{S,TMM}}+Z_{\mathrm{B},\infty}},$$

$Z_{\mathrm{S,TMM}}$ is the impedance of the multilayer seen from the excitation side (computed using the TMM), and $Z_{\mathrm{B},\infty} = k_0 Z_0/\sqrt{k_0^2-(k_x^2+k_y^2)}$ is the radiation impedance [8], seen from the excitation side, k_0 is the acoustic wavenumber, Z_0 is the characteristic impedance in the emission domain, and S is the surface of the multilayer.

Below the critical frequency of the main structure, the wave approach leads to poor results when calculating the sound radiated by a mechanically excited planar structure [8]. However, the transfer matrix method can be extended easily to take into account the panel's size and corrections for the radiation efficiency at low frequencies. The approach proposed by Atalla et al. [9], known under the name of finite transfer matrix method (FTMM) is used here. The application of this method to the calculation of the radiated power is shown by the following equation:

$$\Pi_{\mathrm{rad}} = \frac{1}{8\pi^2}\mathrm{Re}\left[\int_0^{2\pi}\int_0^{+\infty}\frac{Z_0\sigma_{\mathrm{finite}}(k_r,\phi)}{|Z_{\mathrm{S,TMM}}+Z_{\mathrm{B},\infty}|^2}k_r\,dk_r\,d\phi\right] \tag{5}$$

where k_r and φ represent the wave-number and heading in wave-number space, respectively. The "finite size" radiation efficiency is defined by [9]

$$\sigma_{\mathrm{finite}} = \frac{\mathrm{Re}(Z_R)}{Z_0 S} \tag{6}$$

with

$$Z_R = j\omega\rho_0\int_S\int_S \exp[-j(k_x x_0+k_y y_0)]G(M,M_0)\exp[j(k_x x+k_y y)]dS(M_0)dS(M) \tag{7}$$

This term represents a geometrical correction to account for the finite size effect. It depends only on the geometry of the panel. $G(M,M_0)=\exp[-jk_0R]/2\pi R$ is the half space Green's function. The basic idea of this approach is to replace the radiation efficiency in the receiving medium $\sigma_{\mathrm{infinite}}$ by the theoretical baffled radiation efficiency of the window under vibration due to forced propagating waves σ_{finite}. Note that a variant to Eq. (6), in wave-number domain, is the spatial windowing technique of Villot et al. [5].

For airborne excitation, the FTMM has been shown to predict the low frequency transmission loss of complex planar multi-layer system extremely well [9]. This paper will show the importance and the accuracy of this approach for mechanical excitations. However, for the latter the evaluation of the radiated power, using a direct implementation of Eqs. (5)–(7) is computationally expensive. It is shown using analytical integration that the evaluation of Eq. (7) can be reduced to a single integral leading to quick computation of σ_{finite} for a given wavenumber. This in turn speeds up enormously the computation of the radiated power.

2.2. Sea-based approach

In the second approach, based on SEA equations for the main structure, a light coupling is assumed between the structure and the sound package. The effect of the sound package will simply be represented by an equivalent damping η_{eq}. If needed, a mass correction can also be added to the main structure.

At a given frequency, the dispersion equation of the bare panel (plate, solid, composite, etc.) as shown by Eq. (8), is solved for the propagation bending wave-number

$$D_{\mathrm{BarePanel}}(\omega,\varphi) = 0 \tag{8}$$

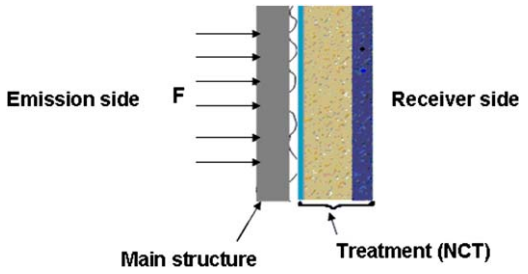

Fig. 2. Panel with acoustic treatment excited with a random force in SEA approach.

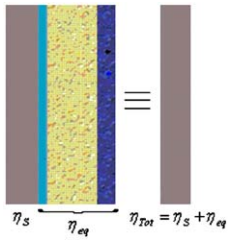

Fig. 3. Multilayer assimilated to the panel in SEA approach.

The latter is imposed to the excited face of the sound package with a pressure-release condition on the rear face, as illustrated in Fig. 2. The TMM is then used to calculate the equivalent added damping using the classical SEA power balance equation:

$$\eta_{\mathrm{eq}} = \frac{\Pi^{t}_{\mathrm{input}}}{\omega M \langle V_1^2 \rangle} \tag{9}$$

where Π^{t}_{input} is the power input to the noise control treatment, calculated using the TMM.

$$\Pi^{\mathrm{t}}_{\mathrm{input}} = \frac{1}{2}|V_1|^2 \mathrm{Re}\left(\frac{Z_0 T_{11} + T_{12}}{Z_0 T_{21} + T_{22}}\right) \tag{10}$$

and V_1 is the velocity of the main structure.

The response of the treated panel is finally recovered from the SEA response of the bare panel using the total damping $\eta_{\mathrm{Tot}} = \eta_{\mathrm{s}} + \eta_{\mathrm{eq}}$ (Fig. 3). Here η_{s} denotes the structural damping of the main structure. In the case of a strong coupling (e.g. viscoelastic treatment, rigid foam, etc.), it is necessary to include these layers in the main structures by calculating the equivalent properties.

2.3. Modal approach

The same methodology is used for the modal approach (third approach). The response of the main structure is written in terms of its modes, and the effect of the sound package on each mode (m,n) is replaced by a modal impedance $Z_{mn,\mathrm{NCT}}$, which is calculated using the TMM with a trace wavenumber $k_{t,mn}$. Once again, it is assumed in this calculation that the receiver face of the multilayer is a pressure-release surface and modal damping is used in the modal impedance expression (as a modal structural damping) and is considered constant (equal for all modes). The total modal impedance is written as

$$Z_{mn,T} = Z_{mn(\mathrm{Bare\ Panel})} + Z_{mn,\mathrm{NCT}} \tag{11}$$

where $Z_{mn(\mathrm{BarePanel})}$ is the modal impedance of the bare panel. $Z_{mn,\mathrm{NCT}}$ is calculated by solving the equation of motion of the system illustrated by Fig. 4

$$Z_{mn(\mathrm{BarePanel})} V_{mn} = F_{mn} - \int_S P_{\mathrm{interface}}(x,y)\phi_{mn}(x,y)\,dx\,dy \tag{12}$$

where $P_{\mathrm{interface}}$, $\varphi_{mn}(x,y)$, V_{mn}, F_{mn} are the panel-treatment interface pressure, the panel's mode shapes, modal velocity and generalized force, respectively.

$Z_{mn,\mathrm{NCT}}$ is related to $P_{\mathrm{interface}}$ via following relation:

$$Z_{mn,\mathrm{NCT}} V_{mn} = \int_S P_{\mathrm{interface}}(x,y)\phi_{mn}(x,y)\,dx\,dy \tag{13}$$

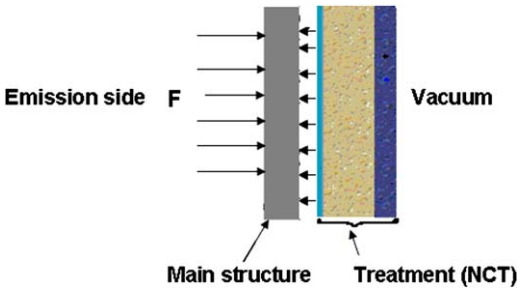

Fig. 4. The pressure exerted by the treatment on the plate in modal approach.

Expanding $P_{\text{interface}}$ in terms of the panel's mode shapes

$$P_{\text{interface}}(x,y)=\sum_{m,n}P_{mn}\varphi_{mn}(x,y) \tag{14}$$

and using orthogonality of the modes, one finally obtains the expression of the sound package modal impedance matrix:

$$Z_{mn,\text{NCT}}=\frac{P_{mn}}{V_{mn}}N_{mn} \tag{15}$$

where $N_{mn}=S/4$ is the modal norm for simply supported panel and S is the surface of the panel. The ratio P_{mn}/V_{mn} is obtained from the condensed transfer matrix of the sound package, Eq. (2). Assuming a pressure-release condition at the rear face, the general form of Eq. (15) is given by Eq. (16)

$$Z_{mn,\text{NCT}}=\frac{T_{12}}{T_{22}}N_{mn} \tag{16}$$

Finally, the space averaged quadratic velocity and the acoustic power radiated by the panel are given by

$$\langle V^2\rangle=\frac{|F|^2}{32}\sum_{m,n}\frac{1}{|Z_{mn(\text{BarePanel})}+Z_{mn,\text{NCT}}|^2} \tag{17}$$

$$\Pi_{\text{rad}}=\rho_0 c_0 S\frac{|F|^2}{32}\sum_{m,n}\frac{\sigma_{mn}}{|Z_{mn(\text{BarePanel})}+Z_{mn,\text{NCT}}|^2} \tag{18}$$

Here, σ_{mn} denotes the modal radiation efficiency of the panel. The asymptotic formulation of Leppington [10] is used in the numerical examples shown in this paper.

3. Numerical results

This section describes several examples illustrating the application and the validity of the three presented approaches in two configurations: single-wall and double-wall. The single-wall is studied using a plate with an attached layer in two situations light and strong coupling (fibrous materiel and elastic foam); whereas, the double wall is investigated using three cases: plate–fibrous material–plate system, plate–elastic foam–plate system and a sandwich panel covered by a foam (elastic porous) and septum (mass layer).

In order to validate the three approaches, a systematic comparison with the finite element method is presented. The comparison is shown for the quadratic velocity and radiated power on both sides of the structures. The finite element method prediction is carried out with an in-house finite element prediction code. The plates were modeled using linear elements with four nodes and the foam is modeled using quadratic porous elements with eight nodes. The (u,p) formulation presented by Atalla et al. [11] is used for the modeling of the porous layers. Finally, the damping is included directly in the expression of the elastic modulus.

Note that the plates are assumed baffled for acoustic radiation (i.e. use of the Rayleigh integral). Moreover, due to the cost of the FEM calculation, the results are limited to point load excitation and is located at (0.45, 0.45), whereas in the presented approaches the excitation is assumed to be a rain-on-the-roof. In the wave approach, the position of point load has no significance since the structure is infinite and in the modal approach, a point force with random location with equal probability (rain-on-the-roof) is used. Eqs. (15) and (16) assume a theoretical average over all possible locations.

Finally, note that the vibroacoustic response of the receiver side can only be obtained with the finite transfer matrix approach (first approach) and due to the nature of the used methods; all the presented results are frequency band averaged using one-third octave bands.

The first stage of numerical calculation is to study the convergence, in other words, to establish how many elements (mesh for the finite element method), expansion order for the modal method and approximation of the infinite integration over wavenumber for the finite transfer matrix method. For the finite element method, the mesh was guided by the

smallest wavelengths in the modeled components (use of 6 linear elements per wavelength) and successive refinement of the mesh used to verify convergence. A similar approach is used for the modal approach (i.e. modes with natural frequency up to 1.5 times the maximum frequency of interest were kept and successive increase of the number of kept modes used to validate convergence). For the wave approach, it was found that integration up to $40\,k_0$ was sufficient for convergence of the results. In this latter approach, Gauss–Kronrod adaptive numerical integration was used to evaluate the integrals.

The first example consists of a $1\,m \times 1\,m \times 0.003\,m$ bare aluminum panel excited by a point load. A comparison of the quadratic velocity, computed using the three presented approaches and the FEM, is given in Fig. 5. An excellent agreement is observed. The FEM depicts modal fluctuations at lower frequencies (recall that data is presented in 1/3 octave bands).

To compare various estimations of the radiated power, the calculations are done using (i) a geometrical correction (FTMM) in the wave approach, (ii) the asymptotic expressions of the radiation efficiency developed by Leppington [10] in the SEA and modal approaches and (iii) the Rayleigh integral in the FEM. The results are shown in Fig. 6. For illustration purposes, the radiated power computed by the TMM (infinite panel radiation efficiency) is also shown. As expected the TMM mainly captures the radiated power above the critical frequency. However, using the FTMM, good agreement is observed over the whole frequency range. In this simple case (bare panel), the excellent agreement observed between the three presented approaches and FEM is expected. Still the results are interesting since they demonstrate the relevance of the simple size correction used in the FTMM for calculating the radiated power.

Next, the case of single-wall is presented with two configurations: light coupling represented by a $1\,m \times 1\,m \times 3\,mm$ aluminum panel with an attached 3 cm thick fibrous material and strong coupling by replacing the fibrous material with 3 cm thick elastic foam. The properties of the fibrous material and the foam are given in Table 1.

A mesh of $50 \times 50 \times 6$ linear brick poroelastic elements is used for the fibrous material and foam. These meshes have been selected to ensure convergence of calculations. Figs. 7–10 show comparison of the various methods for the quadratic velocity and radiated power in the emission side.

Good agreement was observed between the three approaches and FEM. The FEM and modal approach depict modal fluctuations at lower frequencies due to their modal character.

The comparison of radiated power in emission side is also good keeping in mind the assumptions made for the different methods used to estimate the radiation efficiency (Figs. 9 and 10). The results also corroborate the validity of the FTMM in estimating the radiation efficiency compared to the classic methods of Leppington [10] and direct evaluation of the Rayleigh integral.

The first double-wall configuration consists of a flat $1\,m \times 1\,m \times 0.001\,m$ aluminum panel with 3 cm thick attached fibrous material/foam covered with a 2.44 mm septum. Figs. 11 and 12 show the comparison of quadratic velocity in the emission side using the FTMM, SEA, modal approaches and FEM.

For both light coupling (limp fibrous material) and strong coupling (bonded foam) good agreement is observed. The tendencies are well captured and all methods were able to capture the mass-spring-mass resonance of the system for the

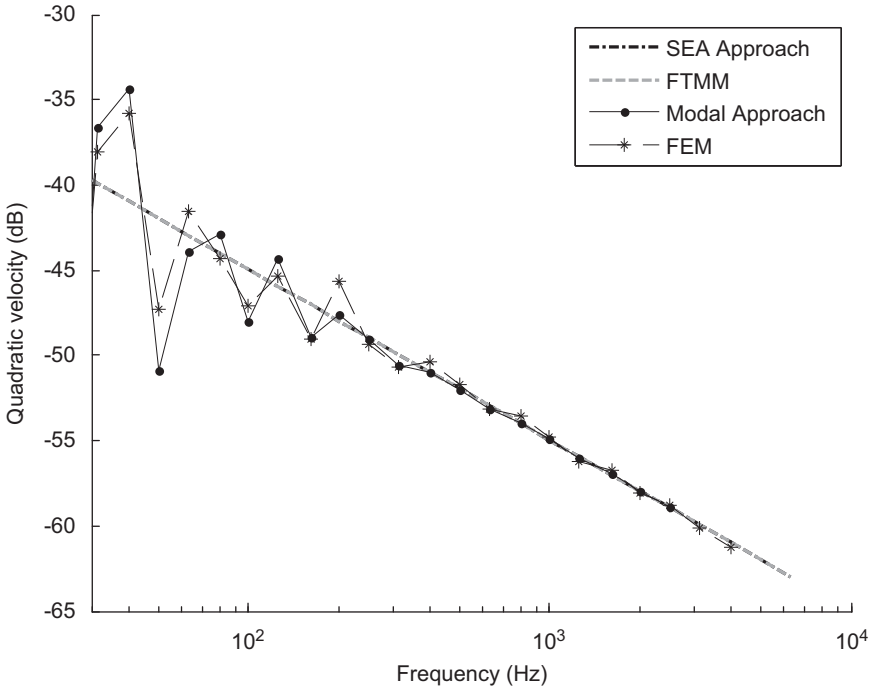

Fig. 5. Quadratic velocity of a bare aluminum panel (dB re 1 m/s).

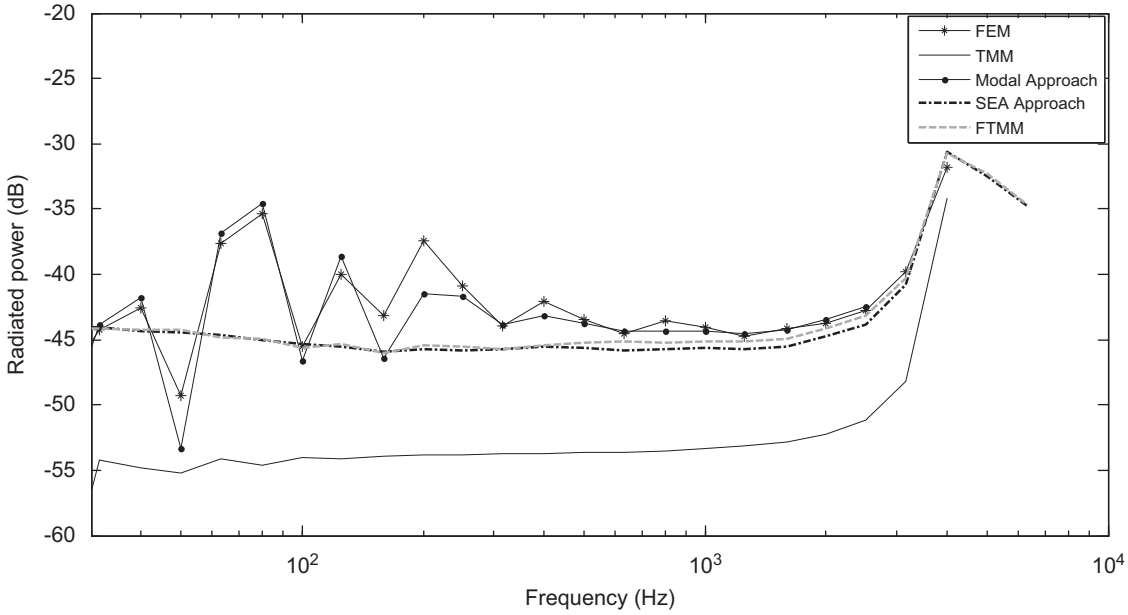

Fig. 6. Radiated power of a bare aluminum panel (dB re 1 watt).

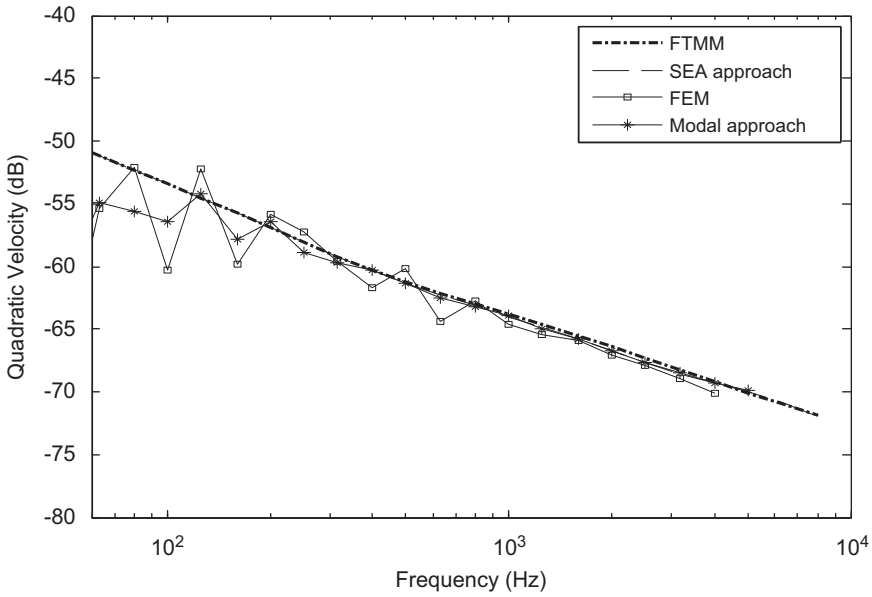

Fig. 7. Quadratic velocity of a plate–fibrous material system (dB re 1 m/s) (emission side).

strong coupling case. However, in the latter, both SEA and the FTMM overestimate the response at low frequencies which is understandable considering the assumptions of both methods. Note that in the SEA approach the mass effects are included via a smeared added mass but the effects of the stiffness are neglected.

To illustrate the accuracy of the estimation of the radiated power, Fig. 13 shows the radiated power in the receiver side for the strong coupling configuration. Recall that as presented only the FTMM is able to calculate the vibration and acoustic indicators on the receiver side. Again, good comparison is observed between the FEM and the FTMM. The latter takes a fraction of the set-up and computation time needed for FEM.

In the last double-wall example, we consider the panel-foam-septum case and replace the steel panel by a highly damped panel (typical metal polymer sandwich panel: MPS). This case depicts strong coupling, and, thus, the direct use of the presented SEA approach will be expected to fail. Tables 1 and 2 give the properties of the studied configurations. Since

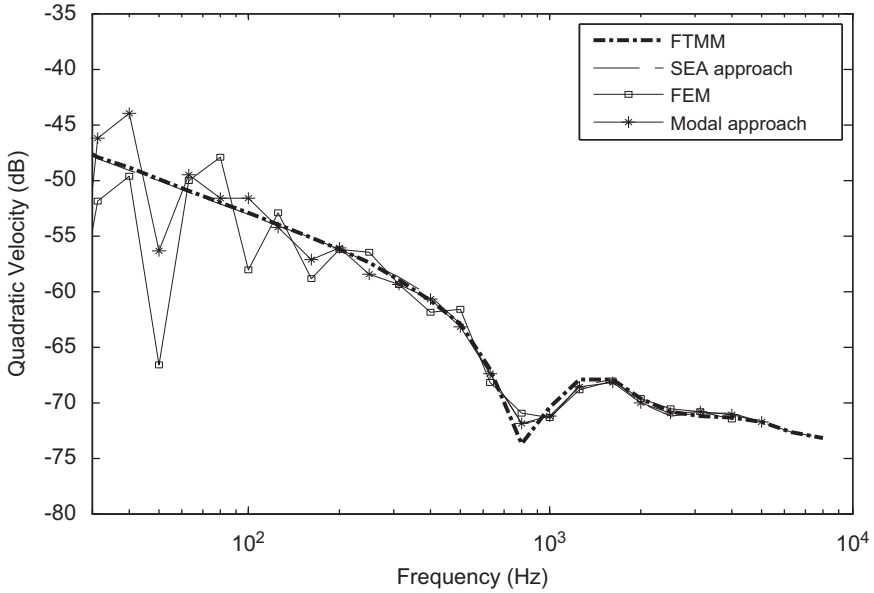

Fig. 8. Quadratic velocity of a plate–foam system (dB re 1 m/s) (emission side).

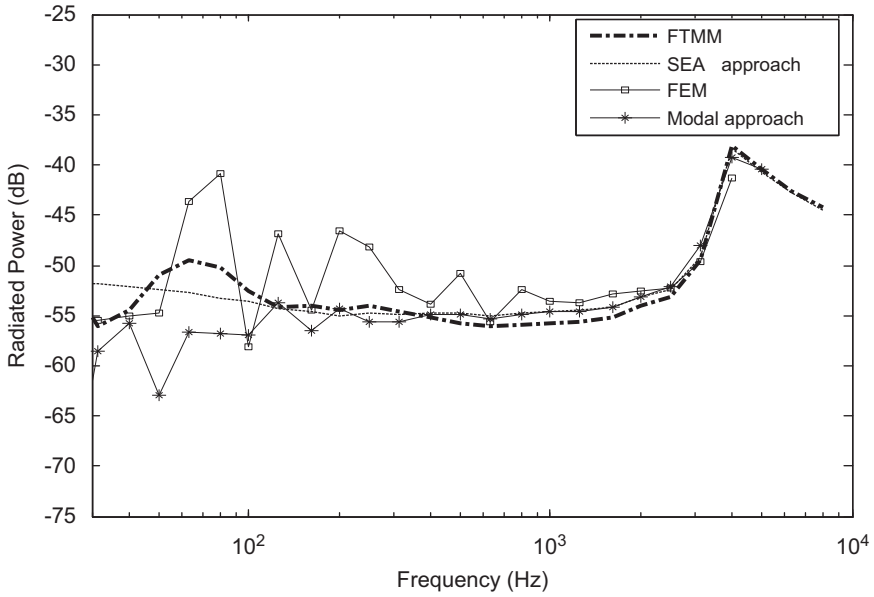

Fig. 9. Radiated power of a plate–fibrous material system (dB re 1 watt) (emission side).

frequency dependency of the viscoelastic layer's properties is of no interest here, the loss factor and Young's modulus of the added layer are assumed to be frequency independent. Still, representative values are used. The MPS panel is modeled using three solid layers in the FTMM. In SEA and modal approaches equivalent properties are used for the MPS panel using an isotropic laminate model [12]. Other models such as Ross-Kerwin-Ungar [13], sandwich model and general laminate model [12] could have been used but they lead to similar results. Finally, a sandwich finite element was used in the FEM predictions. This element has been proven to lead to similar results compared to the classical but costly solid element modeling [14].

Figs. 14 and 15 show the results for the quadratic velocity of the panel and power radiated by the system into the receiver domain, respectively. As expected the SEA approach overestimates the quadratic velocity below the double wall

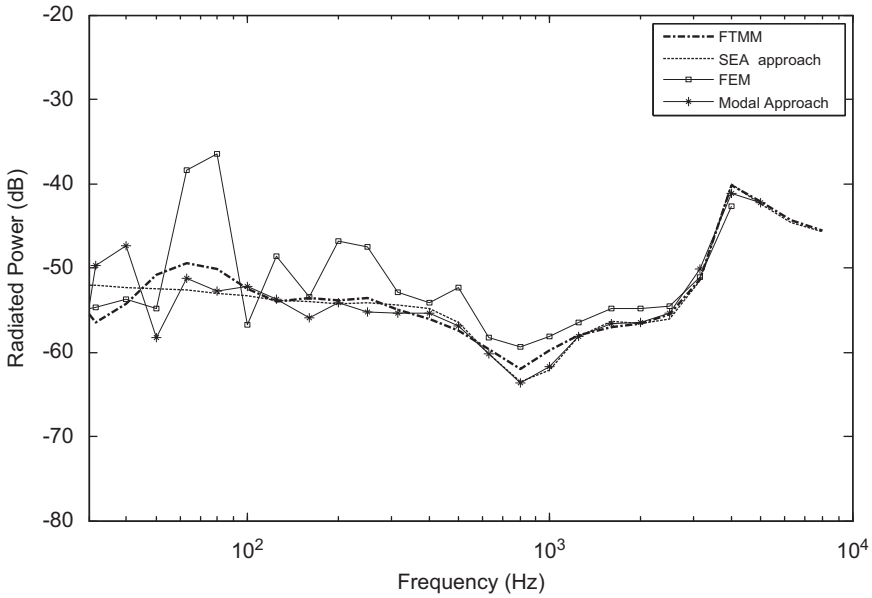

Fig. 10. Radiated power of a plate–foam system (dB re 1 watt) (emission side).

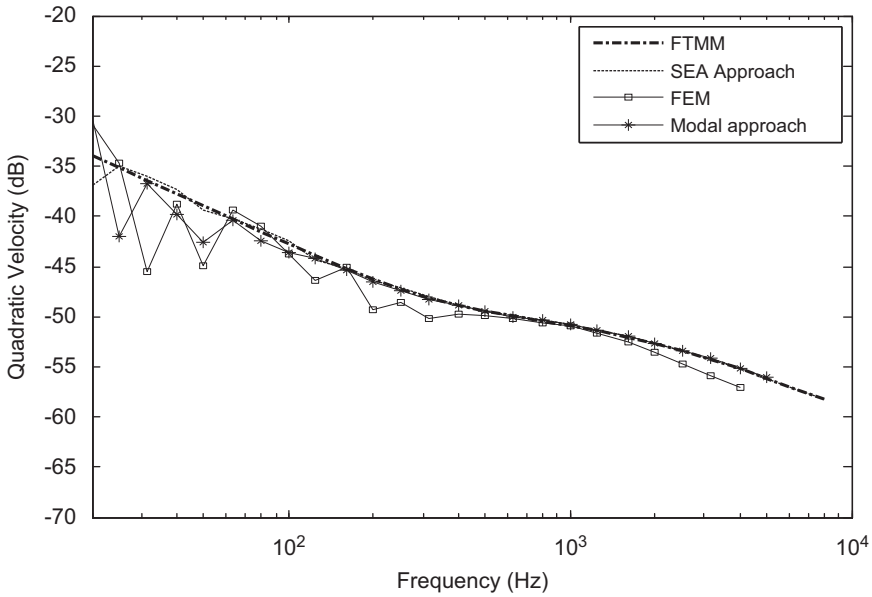

Fig. 11. Quadratic velocity of a plate–fibrous material–plate system (dB re 1 m/s) (emission side).

resonance of the system but overall leads to good predictions. On the other hand, the FTMM and the modal methods lead to excellent results. On the receiver side, the FTMM overpredicts the power radiated compared to FEM but the tendencies are well captured. This is however acceptable keeping in mind the assumptions made for the methods used to estimate the radiation efficiency in both methods. Again, these results are obtained at a fraction of the cost needed for the FEM computation.

4. Airborne and structure-borne insertion loss

Finally to illustrate a practical application of the presented FTMM method, airborne insertion loss (ABIL) and structure-borne insertion loss (SBIL) are compared for two typical sound packages added to a panel. ABIL is classically used to

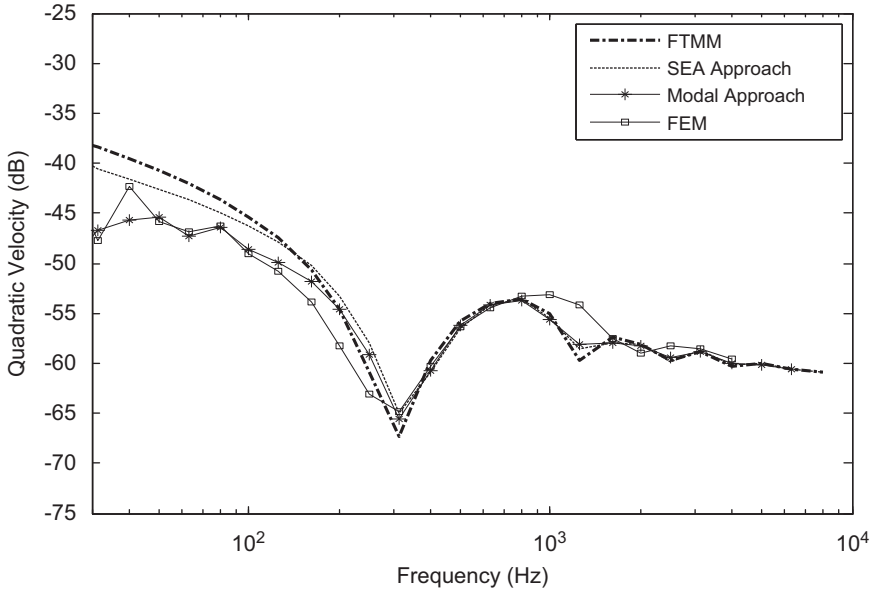

Fig. 12. Quadratic velocity of a plate–foam–plate system (dB re 1 m/s) (emission side).

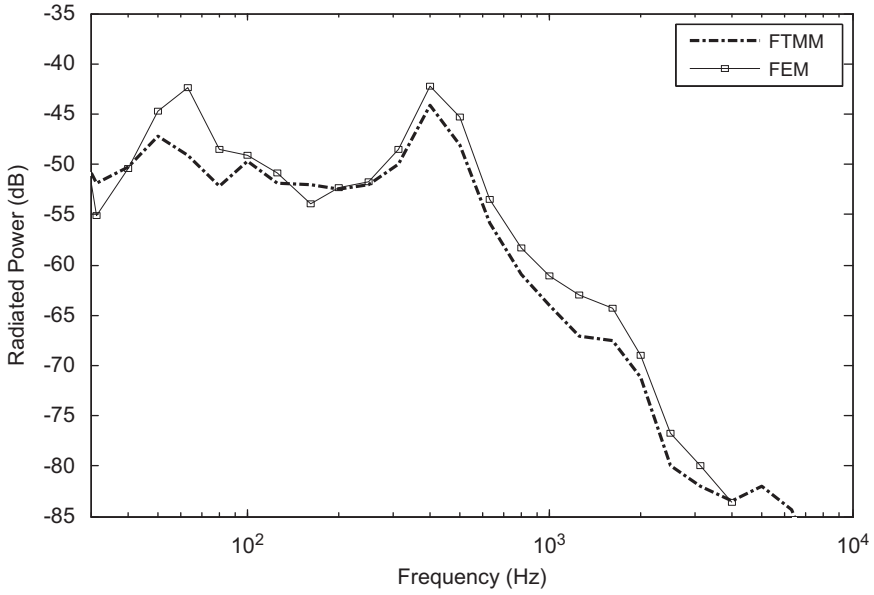

Fig. 13. Radiated power of a plate–foam–plate system (dB re 1 watt) (receiver side).

compare the performance of sound packages. It is also widely used in SEA models to account for the effects of acoustic materials [15]. It is given by the difference of the transmission loss (TL) of the bare and treated panel (Fig. 16 (a))

$$\mathrm{ABIL} = (\mathrm{TL})_{\mathrm{treated}} - (\mathrm{TL})_{\mathrm{bare}} \tag{19}$$

where

$$\mathrm{TL} = 10\log_{10}\left(\frac{\Pi_{\mathrm{inc}}}{\Pi_{\mathrm{trans}}}\right) \tag{20}$$

Here Π_{inc} and Π_{trans} denote the incident and transmitted power, respectively.

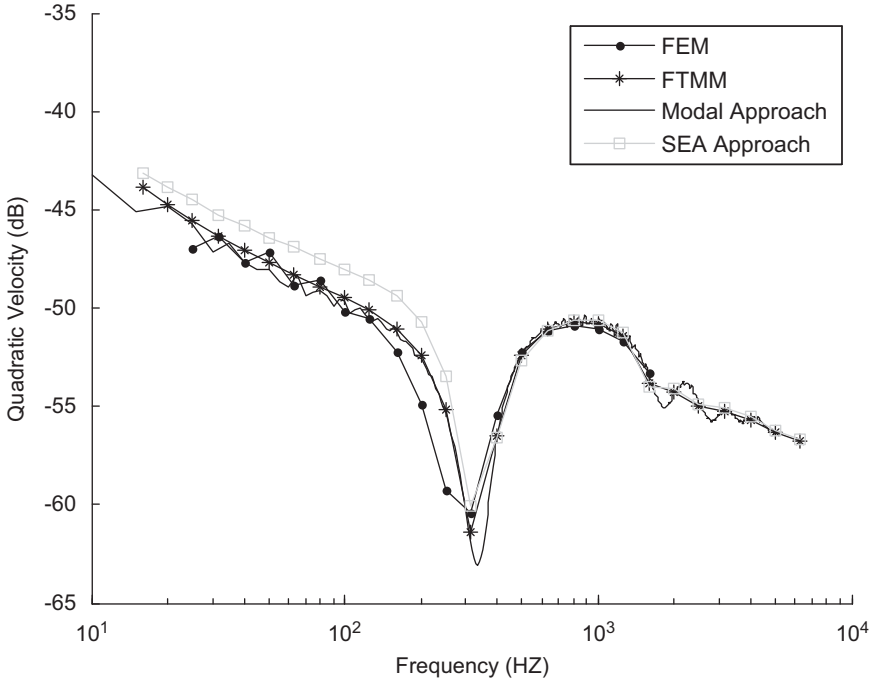

Fig. 14. Quadratic velocity of a MPS–foam–septum system (dB re 1 m/s) (emission side).

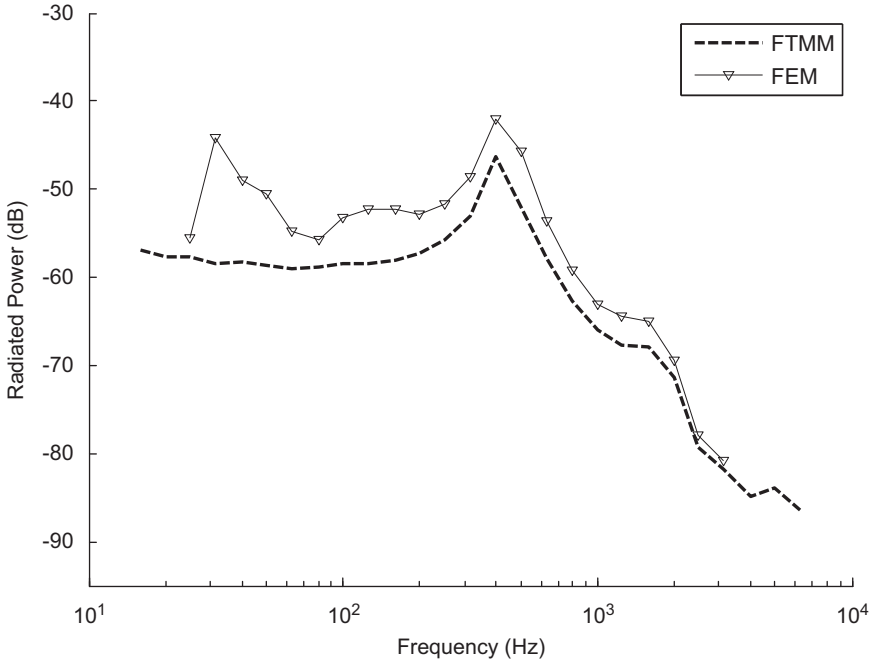

Fig. 15. Radiated power of a MPS–foam–septum system (dB re 1 watt) (receiver side).

For several applications, the question arises about the validity of using the ABIL in SEA models where resonant behavior is dominant or in configurations where a mechanical excitation is used.

Nelisse et al. [7] show experimentally that the airborne insertion loss and the structure-borne insertion loss are very similar for highly damped panels. The differences are mainly limited to low frequencies. Structure-borne insertion loss is defined here, [16], by subtracting the acoustical-mechanical conversion efficiency $(AMCE)_{bare}$ for a bare flat steel plate from

Table 1
Characteristics of the fibrous material and foam.

	Fibrous material	Foam
Dimensions $L_x \times L_y \times h$ (m)	$1 \times 1 \times 0.03$	$1 \times 1 \times 0.03$
Fluid phase density ($kg\,m^{-3}$)	1.213	1.213
Fluid phase sound speed ($m\,s^{-1}$)	342.2	342.2
Porosity	0.99	0.98
Flow resistivity ($N\,s\,m^{-4}$)	1.8×10^4	2.2×10^4
Tortuosity	1	1.9
Viscous characteristic length (m)	6.0×10^{-5}	8.7×10^{-5}
Thermal characteristic length (m)	1.2×10^{-4}	1.46×10^{-4}
Mass density ($kg\,m^{-3}$)	6	30
Young's modulus (Nm^{-2})	0	29×10^4
Poisson ratio	0	0.2
Structural damping	0	0.18

Table 2
Characteristics of the MPS panel.

	Layer 1	Core	Layer 2
Dimensions $L_x \times L_y \times h$ (m)	$1 \times 1 \times 0.00045$	$1 \times 1 \times 10^{-4}$	$1 \times 1 \times 0.00045$
Young's modulus ($N\,m^{-2}$)	2.1×10^{11}	1×10^6	2.1×10^{11}
Density ($kg\,m^{-3}$)	7800	7000	7800
Poisson ratio	0.28	0.49	0.28
Damping	0.007	0.3	0.007

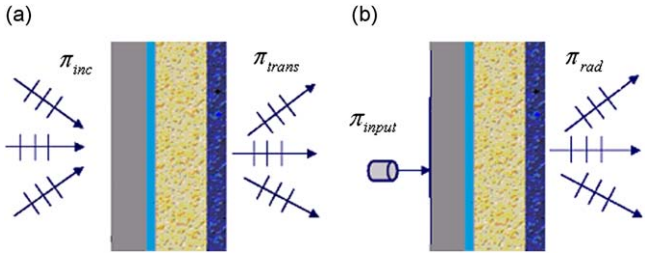

Fig. 16. (a) Airborne and (b) structure-borne configurations.

the $(AMCE)_{treated}$ of the same plate covered with the noise control treatment (Fig. 16 (b)). The latter is calculated from the force and velocity at the excitation point. It is important to use the real part of the complex product which stands for the input energy (effective power).

$$SBIL = (AMCE)_{treated} - (AMCE)_{bare} \tag{21}$$

where

$$AMCE = 10 \log_{10}\left(\frac{\Pi_{input}}{\Pi_{rad}}\right) \tag{22}$$

Here Π_{input} and Π_{rad} denote the input and radiated power, respectively.

In this section, these two indicators are compared for the two double-wall configurations of the previous section: panel-foam-septum and MPS-foam-septum. In both cases, the mechanical excitation is modeled using randomly positioned point loads (rain-on-the-roof) and the acoustic excitation by a diffuse field. As mentioned previously, among the three presented methods, only the wave approach is able to compute the radiated power into the receiver side and thus the structure-borne insertion loss using Eq. (19).

The results are shown in Figs. 17 and 18 for the lightly damped and highly damped structures, respectively. For the lightly damped system (the model still accounts for the damping added by the sound package) it is observed that the two indicators, while showing the same tendencies, are different over the whole frequency range. The difference is mainly important near the double wall resonance of the system. The difference between the two indicators diminishes with the damping of the main structure (Fig. 18). For the presented case, the two indicators are similar at low frequencies and close at high frequencies. The difference at high frequencies is however somewhat surprising since one may expect the two indicators to be close as frequency increases. The obtained results (Fig. 18) were however corroborated by the FEM

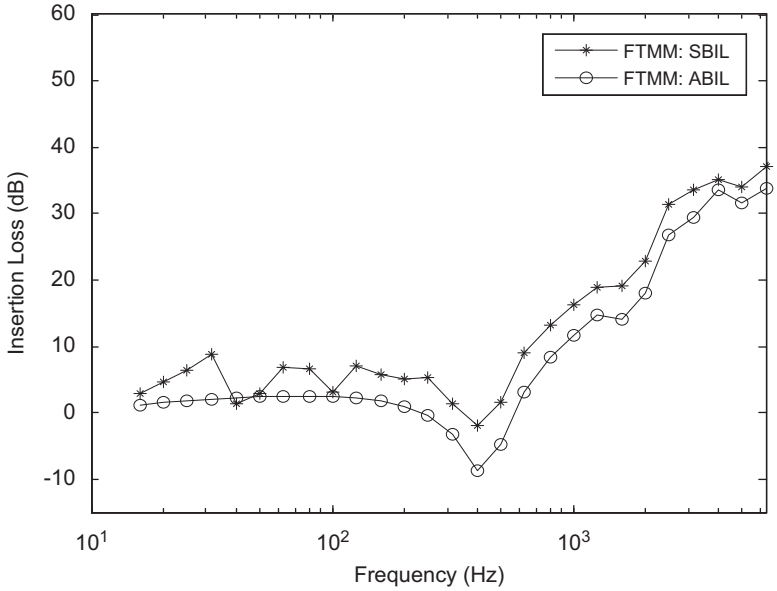

Fig. 17. Comparison between the SBIL and ABIL for a panel–foam–septum system.

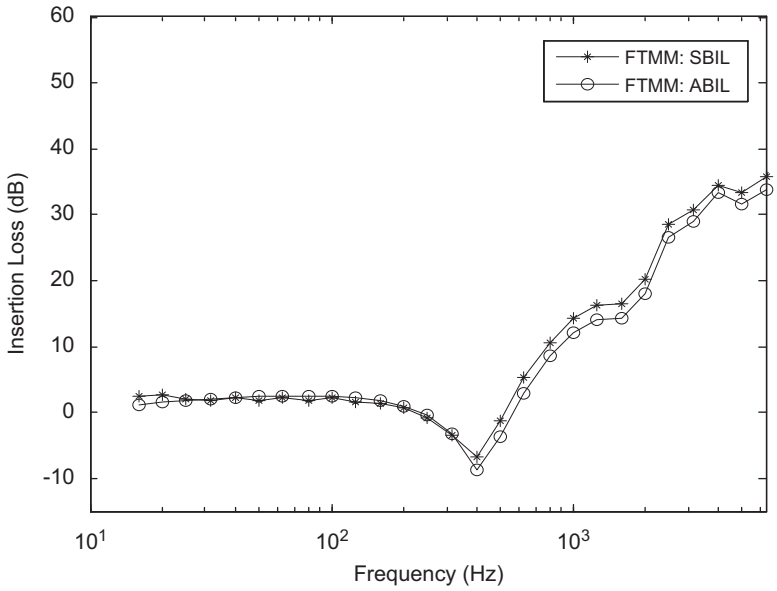

Fig. 18. Comparison between the SBIL and ABIL for a MPS–foam–septum system.

simulations. Note that the same comparison, not shown here, has been done between indicators for single-wall configuration. However, this time, the two indicators are similar at high frequencies and mainly differ at low frequencies, especially for the undamped structure. These results are in line with the experimentally observed similarity between airborne insertion loss and structure-borne insertion loss for damped systems [7]. This also justifies somehow the current SEA practice, which uses ABIL to correct both the resonant and non-resonant transmission paths in a panel with an attached sound package under various excitations.

The physical interpretation of the comparison between structure-borne insertion loss and airborne insertion loss is as follows.

In the case of acoustically excited structures the forced wave motion is dominant. Whereas, in the case of mechanically excited structures it is the resonant wave motion that controls the response. Hence, the difference between airborne insertion loss and structure-borne insertion loss is mainly due to these two phenomena. In the presence of the damping of

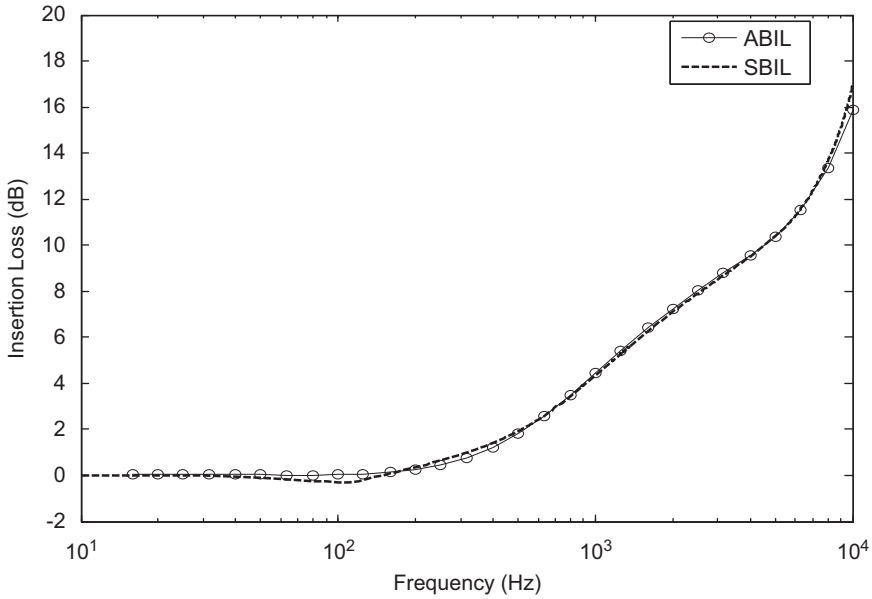

Fig. 19. Comparison between the SBIL and ABIL for an infinite plate–fibrous material system.

the main structure, the maximum magnitude of the resonant waves is reduced and the forced wave motion is established. For this reason the difference between airborne insertion loss and structure-borne insertion loss diminishes with damping.

Note that, if the system finite size was not taken into account, the two indicators will be similar (we have verified that the two indicators are equal (e.g. see Fig. 19 for single-wall configuration)). However, as explained in the text, ignoring the finite size effect is erroneous for the structural excitation at low frequencies. This equality of the two indicators when finite size is ignored confirms actually the interpretation given above. Without the finite size correction, the used radiation efficiency is based on the infinite panel expression which does not capture correctly the radiation of the system below its critical frequency. For a diffuse acoustic field excitation, this is acceptable (for the calculation of the insertion loss) since the transmission is governed by mass (non resonant) while for a mechanical excitation this is not the case since the response below the critical frequency is governed by waves propagating at subsonic speeds. Actually, below the panel's critical frequency, the main contributor to the radiated power in the integral over wavenumber in Eq. (5) is obtained for waves with a wavenumber greater than the acoustic wavenumber. This dominant contribution is simply ignored when finite size effect is not accounted for since the real part of $Z_{B,\infty}$ in Eq. (4) is nil.

5. Conclusion

Three simple methods are presented and compared for the quick estimation of the structure-borne response of finite size flat structures with added sound packages. A systematic comparison with the FEM for various single-wall and double-wall configurations show that these methods represent an attractive alternative to finite element methods for quick assessment of sound package performances. The three methods are shown to work correctly when used within their assumptions. However, the wave approach (FTMM) represents the best methodology since it eliminates the assumption of low coupling assumed in the two other methods. Moreover, it allows for an efficient computation of both the airborne insertion loss and the structure-borne insertion loss of sound packages.

Acknowledgements

The authors thank the FQRNT (Fonds québécois de la recherche sur la nature et les technologies) for their financial support.

References

[1] D.L. Folds, C.D. Loggins, Transmission and reflection of ultrasonic waves in layered media, *Journal of the Acoustical Society of America* 62 (5) (1977) 1102–1109.
[2] J.F. Allard, N. Atalla, *Propagation of Sound in Porous Media: Modeling Sound Absorbing Materials*, vol. 2e, John Wiley & Sons Ltd, 2009.
[3] B. Brouard, D. Lafarge, J.F. Allard, A general method of modeling sound propagation in layered media, *Journal of Sound and Vibration* 183 (1) (1995) 129–142.

[4] N. Atalla, An overview of the numerical modeling of poroelastic materials, Congress Symposium on the Acoustics of Poro-Elastic Materials, France 2004.
[5] M. Villot., C. Guigou-Carter, L. Gagliardini, Predicting the acoustical radiation of finite size multi-layered structures by applying spatial windowing on infinite structures, *Journal of Sound and Vibration* 245 (3) (2001) 433–455.
[6] C. Guigou-Carter, M. Villot, J.L. Kouyoumji, *Analytical and Experimental Study of Wood Floorings*, Forum Acusticum, Budapest, 2005.
[7] H. Nelisse, T. Onsay, N. Atalla, Structure-borne insertion loss of sound package components, Society of Automotive Engineers paper 03NVC-185, Traverse City, Michigan, 2003.
[8] F. Fahy, *Sound and Structural Vibration Radiation, Transmission and Response*, Academic press, London, 1985.
[9] N. Atalla, F. Sgard, C.K. Amedin, On the modeling of sound radiation from poroelastic materials, *Journal of the Acoustical Society of America* 120 (4) (2006) 1990–1995.
[10] F.G. Leppington, E.G. Broadbent, K.H. Heron, The acoustic radiation efficiency from rectangular panels, *Proceedings of the Royal Society, London* 382 (1982) 245–271.
[11] N. Atalla, M.A. Hamdi, R. Panneton, Enhanced weak integral formulation for the mixed (u,p) poroelastic equations, *Journal of the Acoustical Society of America* 109 (6) (2001) 3065–3068.
[12] S. Ghinet, N. Atalla, H. Osman, The transmission loss of curved laminates and sandwich composite panels, *Journal of the Acoustical Society of America* 118 (2) (2005) 774–790.
[13] A.D. Nashif, D.I.J. Jones, J.P. Henderson, *Vibration Damping*, Wiley, New York, 1985.
[14] K. Amichi, N. Atalla, R. Ruokolainen, An efficient sandwich plate element for predicting the vibro-acoustic response of laminated steel panels, paper NC08-214, Noise-Con, 2008, Dearborn, MI, 28–30 July 2008.
[15] B. Cimerman, P. Bremner, Y. Qian, J.A.V. Buskirk, Incorporating layered acoustic trim materials in body structural acoustic models, *Vibroacoustic Sciences Inc* 104 (2) (1995) 2289–2294 no 6.
[16] L.L. Beranek (Ed.), *Noise and Vibration Control Engineering-Principles and Applications*, Wiley, New York, 1992.